© Med Sci Monit, 2010; 16(8): BR233-245
PMID: 20671603

BR

Received: 2010.03.24
Accepted: 2010.04.12
Published: 2010.08.01

MALDI imaging mass spectrometry in ovarian cancer for tracking, identifying, and validating biomarkers

Authors' Contribution:
A Study Design
B Data Collection
C Statistical Analysis
D Data Interpretation
E Manuscript Preparation
F Literature Search
G Funds Collection

Mohamed El Ayed*[1,2BCD], David Bonnel*[1,3BCD], Remi Longuespée[1,3BF], Céline Castellier[1,4B], Julien Franck[1BD], Daniele Vergara[1B], Annie Desmons[1B], Aurélie Tasiemski[1B], Abderraouf Kenani[2EF], Denis Vinatier[4AG], Robert Day[3EG], Isabelle Fournier[1ADEFG], Michel Salzet[1ADEFG]

* join first authors

[1] Université Nord de France, CNRS, MALDI Imaging Team, Laboratoire de Neuroimmunologie et Neurochimie Evolutives, Université Lille 1, Lille, France
[2] Laboratoire de Biochimie – Unité de Recherches "Mécanismes Moléculaires et Pathologies", Faculté de Médecine de Monastir, Monastir, Tunisie
[3] Institut de Pharmacologie de Sherbrooke, Faculté de Médecine et des Sciences de la Santé, Université de Sherbrooke, Sherbrooke, Québec, Canada
[4] Clinique de Gynécologie, Hôpital Jeanne de Flandre, CHRU Lille, Lille, France

Source of support: Supported by grants from Centre National de la Recherche Scientifique (CNRS), Ministère de L'Education Nationale, de L'Enseignement Supérieur et de la Recherche, Agence Nationale de la Recherche (ANR PCV to IF), Institut du Cancer (INCA to IF), Institut de Recherche en Santé du Canada (ISRC to MS & RD), Région Nord-Pas de Calais (to DB & RL), Fonds de la Recherche en Santé du Québec (FRSQ to RD)

Summary

Background: Among biomarkers, cancer-antigen 125 (CA-125) is the most studied. We propose an analytical tool to track ovarian carcinoma biomarkers, that is, the MALDI mass spectrometry imaging.

Material/Methods: Ovarian carcinomas and benign ovaries were directly analyzed by MALDI-TOF-MS. After automatic profiling and mass spectrometry imaging analyses, hierarchical clustering based on principal component analysis in nonsupervised mode was carried out. On the same samples, preparations were performed to investigate peptides, then proteins, followed by high mass proteins, in an automatic profiling to specific signatures for diagnosis. Using tissue bottom-up strategy on tissue digestion, and mass spectrometry imaging after by shotgun sequencing by nalano-LC-IT-MS in MS/MS mode from washing samples from on tissue digested peptides, several biomarkers were found.

Results: A list of specific biomarkers from the ovarian carcinoma regions was obtained and classified as proteins associated with cell proliferation, involved in immune response modulation, signaling to the cytoskeleton, and tumor progression. These specific biomarkers were then validated by immunocytochemistry using Tag-mass technology, cell biology, Western blot, and by PCR (using SKOV-3 ovarian epithelial cancer cells). A link between the immune regulation (innate immunity, tolerance) and virus cause is also discussed.

Conclusions: From the biomarkers identified, proteins involved in immune response modulation and cell proliferation have been pointed out in this study. Two new markers have been identified using such a strategy, that is, fragment C-terminal of the PSME1 (Reg-Alpha) and mucin-9.

key words: **MALDI imaging • pathologies • innate immunity • proteomics • PCA • hierarchical clustering**

Full-text PDF: http://www.medscimonit.com/fulltxt.php?ICID=881095

Word count: 5539
Tables: 4
Figures: 7
References: 76

Author's address: Michel Salzet, Laboratoire de Neuroimmunologie et Neurochimie Evolutives, FRE CNRS 3249, 59650 Villeneuve d'Ascq, France, e-mail: michel.salzet@univ-lille1.fr

BACKGROUND

Ovarian cancer is the fourth leading cause of cancer death among women in Europe and the United States. Among biomarkers, cancer-antigen 125 (CA-125) is the most studied. CA-125 has a sensitivity of 80% and a specificity of 97% in epithelial cancer (stage III or IV). However, its sensitivity is around 30% in stage I cancer, its increase is linked to several physiological phenomena, and it is also detected in benign situations [1]. CA-125 is particularly useful for at-risk population diagnosis and for following illness evolution during therapeutic treatment. In this context, CA-125 is insufficient as a single biomarker for ovarian cancer diagnosis. Thus, other biomarkers are required to use a proteomic strategy for diagnosis [2–10].

At this time, 2 strategies have been undertaken by researchers. Several, several groups have tried to identify ovarian cancer markers in plasma or serum using SELDI-TOF profiling or chromatography coupled to mass spectrometry [3,11–16]. Other groups have developed a classic proteomic strategy using comparative 2D-gels and mass spectrometry [10,17–19].

Here, we propose another strategy based on direct tissue analysis and peptide profiling followed by MALDI profiling and imaging. Ovarian carcinomas (stages III and IV) and benign ovaries were directly analyzed by MALDI-TOF-MS. Hierarchical clustering based on principal component analysis (PCA) was carried out using ClinProTools software to classify tissues. Principal component analysis was used in the unsupervised mode to differentiate tumorous and healthy spectra based on their proteomic composition as determined by MALDI-MSI. Two stage IV tumor regions as well as 2 healthy regions were identified. To validate the procedure, 2 biomarkers identified in the 2 carcinoma regions were characterized using tissue MS-MS and nanolc-IT-MS. Validation was performed by specific MALDI imaging using the Tag-mass concept, and PCR was performed on mRNA extracted from patients or from an epithelial cancer cell line (SKOV3). The first biomarker was identified as a fragment of the immunoproteasome Reg-Alpha [20], and the second was identified as orosomucoid.

Taken together with recent results from gastric cancer diagnosis [21,22], our results suggest that MALDI-MSI is a promising technology for tumor classification and for identifying specific biomarkers in various types of tumors.

MATERIAL AND METHODS

Materials

α-cyano-4-hydroxycinnamic acid (HCCA), sinapinic acid (SA), 3-acetylpyridine (3AP), 1,1,1,3,3,3-Hexafluoro-2-propanol (HFIP) ammonium bicarbonate (NH_4CO_3), trisma base, xylene, methanol (MeOH), ethanol (EtOH), acetonitrile (AcN), angiotensin II, Des-Arg-bradykinin, substance P, ACTH 18-39, ACTH 7-38, and bovine insulin were obtained from Sigma-Aldrich and used without any further purification. Trypsin was from Promega. AspN, LysC enzyme was from Roche. Trifluoroacetic acid (TFA) was purchased from Applied Biosystems. Acetonitrile p.a. and methanol p.a. were from J.T. Baker.

Samples

Tissues, ascites, and cyst fluids were obtained with informed consent and institutional review board approval (CCPPRBM Lille: CP 05/83) from patients undergoing any ovarian tumor resection at Hospital Jeanne de Flandre. A total of 48 tissue samples from 25 patients with grade III and IV ovarian cancer, and 23 benign tumors, were analyzed. Patient information was collected, including sex, age, treatment received before and after surgery, extent of surgery, current status (alive, alive with progressive disease, deceased, and cause of death), and survival from the time of original pathologic diagnosis. Samples were collected at the time of surgery, immediately frozen, and stored at –80°C until analysis. Typically, 10- to 12-µm thick sections were cut using a cryostat and thaw-mounted on flat, electrically conductive sample slices. Histopathologic diagnoses were made by an anatomopathology blinded to the original clinical diagnosis from subsequent H&E-stained sections.

Tissue preparation

Frozen ovary sections were immediately transferred onto a conductive Indium-Tin Oxide (ITO) glass (Bruker Daltonics, Wissenbourg, France). After drying the sections for 5 minutes at room temperature, tissues were heated to 37°C for 20 seconds to adhere to slides and placed under a vacuum for 10 minutes. They were then rinsed in chloroform and analyzed in MALDI ms for MALDI imaging analyses [23].

MALDI Imaging and Specific MALDI Imaging

Automated tissue profiling

For automated profiling assays, markers of 3 mass ranges were screened for each section. After the tissue treatment, 10 µL of HCCA 10 mg/mL in ACN/TFA 0.1% 7:3 were dropped to perform the analysis of peptides. The laser settings for these analyses were power 40%, offset 65%, range 20%, small focus, and 150 ns of pulsed ion extraction. A methanol 100% wash was then used to remove the matrix, and 10 µL per section of SA 20 mg/mL in AcN/TFA 0.1% were dropped to perform the analysis on the proteins mass range. The laser settings were power 45%, offset 65%, range 20% small focus, and 150 ns of pulsed ion extraction. Ten µL of SA 10 mg/mL in HFIP 100%, then 10 µL of SA 20 mg/mL in ACN/TFA 0.1% 7:3 were then dropped to perform the analysis on high-mass proteins after their extraction from the tissue section [24]. For each analysis, 1000 shots were accumulated for 50 spectra per tissue section.

MALDI Imaging

A solid ionic matrix (sinapinic acid SA/3AP) was prepared just before use and was deposited using a Chemical Inkjet Printing CHIP-1000 device (Shimadzu, Kyoto, Japan) after a raster of spots spaced by 250 µm center to center. Briefly, 4.8 µL (1 equivalent) of 3AP was added to a solution containing 10 mg/mL of SA in ACN/aqueous TFA 0.1% (6/4, v: v). The solution was agitated for several minutes before use. Five droplets of approximately 100 pL were deposed at each spot per cycle. Twenty iterations were necessary to reach the total final volume of 10 nL. Images were acquired using an UltraFlex II MALDI-TOF/TOF instrument

(Bruker Daltonics, Bremen, Germany) equipped with a smart beam laser with a repetition rate of 200 Hz [25] and controlled by FlexControl 2.5 software (Bruker Daltonics). Images were performed in positive reflectron mode and MALDI-MS spectra were acquired in the mass range from 550 to 5000 Da. Six-hundred spectra were acquired at each spot using a laser frequency of 100 Hz. The images were recorded and reconstructed using Fleximaging II 2.5 (Bruker Daltonics) software.

Specific MALDI Imaging

For specific MALDI imaging studies, ovary sections were incubated at room temperature with 500 µL buffer (0.1 M PBS/ 1% BSA / 1% normal goat serum /0.05% triton ×100) for 30 minutes [26,27]. The same buffer was used to dilute the Reg alpha antibody (1/100) (Zymed Laboratories, Invitrogen, ref. 38–2400), and incubation was performed overnight at 4°C. After 3 washes in PBS, sections were incubated overnight with anti-Human IgG photocleavable tagged rabbit antibody (1/100) (Eurogentec) at 4°C [28,29]. The tissues were then rinsed 3 times for 5 minutes with ultrapure water to remove salts, and sections were dried at room temperature before matrix application. In the case of the orosomucoid (alpha 1 glycoprotein) biomarker, a polyclonal antibody (MCA3312Z) was purchased from AbD Serotec and used at a dilution of 1/50. The secondary antibody is an anti-human IgG photocleavable tagged mouse antibody (1/100) (Eurogentec).

Automatic trypsin digestions

The printed array of the CHIP-1000 on the tissue section was composed of spots spaced by 250 µm center-to-center. A total of 40 nL of solution containing 25 µg/mL of trypsin in water was applied to each spot. Five droplets of approximately 100 pL were deposited at each spot per cycle. Forty iterations were necessary to obtain the final volume.

MS/MS of digested and derived tissues

MALDI-TOF MS/MS experiments on digested and derived tissue sections were performed using an Ultraflex II TOF-TOF instrument equipped with a LIFT III cell. For MS/MS experiments, the following parameters were set: laser repetition rate of 100 Hz with 33% attenuation, ion source voltages of 8 kV and 7.3 kV on the MALDI sample plate and first electrode; LIFT cell pulse from ground for electrode 1 and 2 to 19 kV; and in the last step, electrode 3 was decreased to 3.2 kV. Reflector end voltage was set to 29.5 kV and mid-grid to 13.85 kV. For each MS/MS spectrum, 1000 total shots were averaged, including 200 for parent ions and 800 for fragments. Laser fluence was constant over the experiments.

Protein identification in databanks was performed using Biotools 3.0 software (Bruker Daltonics) connected to the Phenyx search engine interrogating the NCBI, Swissprot, EST, or MSDB databases. Methionine oxidation was set as the variable modification, and no fixed modification was used. Taxonomy was specified to be human. Trypsin was selected as the enzyme, and 2 missed cleavages were settled. The mass tolerance was set at 1 and 0.5 Da for the MS and MS/MS.

Bottom-up analyses

Peptide tissue extractions

Slices were washed with acetonitrile (60%) acidified with HCl 1N (w/5v). The collected supernatants were incubated overnight at 4°C with gentle rocking. After centrifugation at 12 000 rpm for 30 minutes at 4°C, the supernatants were loaded on Sep-Pak C18 cartridges (500 µL extract/cartridge; Waters). After washing with 5 mL acidified water (0.05% TFA, Pierce), samples were eluted with 5 mL 60% AcN in acidified water (0.05% TFA). Sixty percent of the eluted fraction was reduced in a vacuum centrifuge (Savant). This fraction was resuspended in 100 µL acidified water (0.05% TFA) and fractionated on a C18 reversed-phase HPLC column (4.6 mm×25 cm, Interchim) equilibrated with acidified water (0.05% TFA). Elution was performed with a linear gradient of acetonitrile in acidified water (0.05%) from 0% to 70% at a flow rate of 500 µL/min. Each fraction was collected manually before being evaporated in a SpeedVac vacuum and resuspended with 50 µL of HPLC grade water. Each fraction was analyzed by MALDI-TOF-MS before trypsin digestion.

Trypsin digestion

After drying, samples (extracted peptides) were placed on ice for 30 minutes in 50 µL of protease solution (sequence grade-modified trypsin, Promega, at 0.02 mg/mL in 25 mM (NH_4HCO_3). Digestion was performed overnight at 37°C. Peptide extraction was performed twice for 15 minutes with 50% acetonitrile, 1% TFA for further MALDI-MS analysis, or with 50% acetonitrile, 1% formic acid for further ESI-MS/MS analysis. Trypsin digests were then lyophilized in a SpeedVac concentrator and resuspended in 5 µL of 0.1% formic acid.

For nanoLC-ESI MS samples

Ten patients with grade III and IV ovarian cancer and 10 benign tumors were analyzed.

The cancer tissue sample contains serous cystadenoma, mucinous cystadenoma, and borderlines tissue.

For nanoLC-ESI MS analysis, on a section of 2 cm^2, *in situ* enzymatic digestion is performed by adding 15 µL of trypsin enzyme (0.033 µg/µL in 25 mM Tris buffer pH 7.4) for 1 hour at room temperature. After enzymatic digestion, purification of resulting digestion peptides was achieved by using reverse phase C_8 coated silica magnetic beads (ClinProts, Bruker Daltonics) according to the protocol of the manufacturer modified for tissues. Then, this, 15 µL of binding solution was directly applied onto the tissue during 1 minute, and then 15 µL of magnetic bead was added on the section. Extraction occurred for 10 minutes. During this step, beads and digested products were mixed 3 times using a micropipette directly onto the tissue. Digestion solution and beads were then deposited in a polypropylene tube and washed 3 times using 500 µL of H_2O/TFA 0.1%. Peptides were eluted from the beads with 30 µL of ACN/H_2O (1:1, v/v) and solution was dried by vacuum centrifugation. For the nano LC-MS/MS identification, peptides were redissolved in H_2O/MEOH 0.1% formic acid (9:1 v/v) after elution and evaporation.

Table 1. Forward and reverse primer sequences used in RT-PCR are shown 5′ to 3′.

Primer designation	Forward primer	Reverse primer
Orosomucoid	CTGGGAGAGTTCTACGAAGC	CCTCCTGTTTCCTCTCCTT
Actin	AGCGCAAGTACTCCGTGTG	GACTGGGCCATTCTCCTTAG
GAPDH	ACCACAGTCCATGCCATCAC	TCCACCACCCTGTTGCTGTA

Nano LC-nanoESI-IT MS and MS/MS

Analyses were performed on an ion trap mass spectrometer (Esquire 3000 plus, Bucker Daltonics) equipped with a nano ESI ion source and on-line coupled to a nano HPLC system. An injection of 0.5 µL of digest was made with a Switchos Autosampler (Dionex corporation) and separation was performed on a C18 silica bonded stationary phase (75 µm id, 150 mm long, 3 µm 100 Å pore size, Dionex). Samples were washed for 2 minutes at 10 µL/min with 100% mobile phase A (95% H_2O, 5% ACN 0.1% formic acid). Peptides were then eluted using a linear gradient of 1%/minute mobile phase B (ACN 80%, H_2O 20%, formic acid 0.08%) for 70 minutes at a flow rate of 0.2 µL/min. The Esquire was operated in a data-dependent MS/MS mode in which 1 MS full scan was followed by 1 MS/MS scan on the most-abundant peptide ion. Collision energy was set to 35%. The heated capillary temperature and electrospray voltage were 160°C and 1.5kV respectively.

Protein identification was performed under MASCOT sequence query search program using SwissProt database filtered for the taxonomy "human." A tolerance of 1 Da for peptide and 0.5 Da for MS/MS was set. Only protein sequences with MOWSE score higher than 20 (indicating significant homology or identity) and identified in several samples representing at least 4 significant MS/MS were considered. Methionine oxidation and acetylation of N – terminal were defined as variable modification.

Statistical data analysis

For statistical analyses, mass spectra were internally recalibrated on common peaks (also known as *spectral alignment*) and normalized to the total ion count. An average spectrum created from all single spectra was used for peak selection and to define integration ranges. These integration ranges were used to obtain the intensities or areas of single spectra. Signal intensities were used for all calculations. For the principal component analysis and hierarchical clustering, the individual peak intensities were standardized across the data set. The Principal Component Analysis (PCA)was carried out using Pareto scaling, which uses the square root of the standard deviation as a scaling factor to reduce the dominance of large-scale intensity changes in the matrix and other high-abundance ions, as these may mask variations in lower abundance ions during PCA. The overall outcome of PCA is greatly affected by the masking of the underlying relevant information by ions related to matrix coating and other endogenous molecules. Under unsupervised PCA, each spectrum is classed as an individual so the principal components are selected and account for the greatest separation of each of the individual spectra.

RNA isolation and PCR analysis

mRNA from biopsies or the SKOV-3 cell line was extracted in 2 mL tubes prefilled with Qiazol reagent (Qiagen, France) and 1.4 mm ceramic beads. The mixture was shaken twice for 45 seconds at 6500 rpm in a Precellys 24 homogenizer (Bertin distributed by Ozyme, France). RNA extraction was performed according to the manufacturer's instructions, and the total extracted RNA was treated with RQ1Dnase1 (Promega, France) to prevent genomic DNA contamination. First strand cDNA was generated from 2 µg of total RNA using random primers (Promega, France) and the Superscript III reverse transcriptase (RT) kit (Invitrogen, France) in a final volume of 60 µL.

Omitting RT or RNA from the reaction mixture resulted in nonamplification and no-template controls. cDNA was treated with RNaseH (Promega, France) to optimize the amplification. For the TLR, Reg-alpha fragment and orosomucoid genes, forward and reverse primers (Table 1) were designed with the Primer3 Input software (*http://frodo.wi.mit.edu/cgi-bin/primer3/primer3_www.cgi*). Toll Like Receptor (TLR) primer pairs were obtained from Krug et al. [29] Actin, GAPDH and 18S were used as reference genes. In each case, PCRs were performed for 30 cycles using Advantage 2 polymerase (Clontech) with an elongation time of 2 minutes. All PCR products were subcloned into the pGEM-T easy vector (Promega) and cDNA clones were sequenced with an ABI Prism 310 genetic analyzer (Applied Biosystems).

qPCR analyses for virus detection genes

Epstein-Barr Virus R-gene quantification kit and CMV HHV6,7,8 R-Gene diagnostic kit (CE-IVD labeled are purchased at Argene and performed on Applied Biosystems 7500 as recommended by the manufacturer.

SKOV-3 cells stimulation and immunohistochemistry

The human epithelial ovarian cancer cell line SKOV-3 was grown in RPMI-1640 medium with glutamine, supplemented with 10% FBS, 100 U/mL penicillin, and 100 µg/mL streptomycin. Cells were treated with TGF-β (10 ng mL^{-1}) for 24 hours in the absence of serum (B). Control cells were left untreated (A). For confocal microscopy analysis, cells were fixed for 5 minutes with 3.7% formaldehyde in phosphate-buffered saline (PBS) solution, permeabilized with a 0.1% solution of Triton X-100 in PBS, followed by 30 minutes incubation at room temperature with phalloidin-TRITC (Sigma). Slices were then mounted in glycergol and examined using a confocal microscope (Zeiss LSM 510). Control cells have a typical epithelial-like morphology in culture flask/Petri with the tendency to form dense colonies.

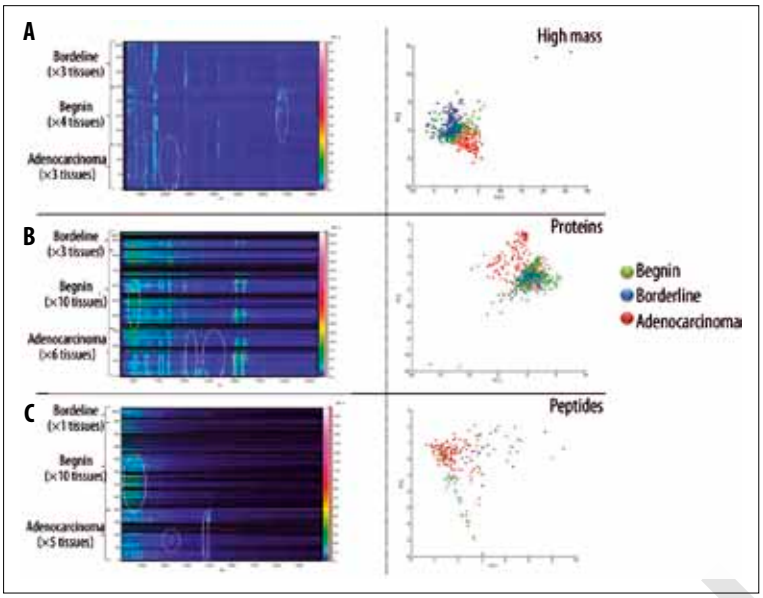

Figure 1. Automatized MALDI profiling on three ovarian tissues classes: adenocarcinoma, borderline and benign. (**A**) Pseudogel and supervised PCA loading plot obtained for a high mass procedure. (**B**) Protein procedure. (**C**) Peptide procedure.

BR

Western blotting

Whole cell lysates (in lysis buffer as described above) containing 50 µg of total proteins (COF1, PROF1) (Sigma) were diluted in cold RIPA buffer, resolved on 12% sodium dodecyl sulphate-polyacrylamide gels (mini protean II electrophoresis system, BioRad) and blotted onto nitrocellulose membranes. The membranes were blocked with 5% w/v nonfat dry milk in TBS containing 0.1% Tween-20 (Sigma) and probed with selected primary antibodies. After incubation with secondary antibodies, immunoblots were visualized with the ECL detection kit (Amersham Biosciences).

Results

Automatic profiling and PCA for biomarkers tracking

Automatic profiling was performed on 20 samples (10 benign, 6 carcinoma, 3 borderline) laid on the same slides and submitted to peptides, then small proteins, and finally high mass proteins tracking using 3 in-house methods, 1 after 1 based on classical matrix deposition and solvent treatments [23,24,30–32]. The analyses of a MALDI imaging data set by molecular mass images can be illustrated as a pseudogel (Figure 1). In peptides conditions (with HCCA as a matrix), carcinoma specific signatures can be found for m/z around 3300 and 4800, whereas in a benign larger zones for m/z ranged from 1200 to 2000 can be found. As can be seen, the borderline profile resembles the benign one. The principal component analysis (PCA) analyses confirm the observation (Figure 1). For small proteins (with SA as matrix), 2 signatures can be seen for m/z comprised between 9500 and 14 000 and 1 around 17 500 in carcinoma samples.

It is difficult to discriminate between borderline and benign profiles except for a specific signature at m/z, ranging between 4900 and 5200 which is, specifically detected in benign samples, and is absent in both carcinoma and borderline profiles (Figure 1). In high-mass proteins, a specific zone comprised between m/z 23 000 and 25 000 in carcinoma whereas in benign and borderline profiles a zone between m/z 65 000 and 68 000 is detected (Figure 1). Principal component analyses (PCA) confirmed the eyes detected zones but 2 others are detected through statistics in carcinoma; that is, 1 around m/z 9000 and 12 000; 1 between m/z 23 000 and 24 000, and the last 1 around m/z 35 000–37 000 (Figure 1). In a borderline profile PCA analyses detected a zone between m/z 5300 and 5000 and in begin a cross-zone with the malignant 1 at m/z 10 000 and 11 000 (Figure 1).

All together, the data shows that it is necessary to perform on same samples the 3 procedures, helped with PCA analyses to have a clear overview of different classes of biomolecules present in the samples and to drive the biomarker hunting. In this context, as it can be seen in Figure 1B, a classic procedure using SA as matrix for peptides and small proteins did not allow one to detect high-mass proteins, only polar ones can be obtained. Thus, the HFIP procedure [24] was applied, and the number of peaks detected in the *m/z* 20 000 to 50 000 range was clearly increased (Figure 1A). Interestingly, several of these peaks are consistent with previously identified biomarkers using classic 2D proteomic procedures (Table 2), suggesting that the chemical treatments could enable known biomarkers to be recorded directly from tumor regions in tissue biopsies. These show that MSI can be more complementary to the classic proteomic for biomarker tracking.

MALDI Imaging Mass Spectrometry and Principal Component Analyses for biomarkers tracking

MALDI imaging mass spectrometry analyses were performed on carcinomas tissues (stage III or IV) followed by PCA analyses using SA/3AP as matrix (Figure 2A). Unsupervised PCA was used to attempt to identify hidden variables between spectra taken from various regions of ovarian biopsy (Figure 2B). Figure 2B shows the score plots for unsupervised PCA. Plot PC1/PC2 shows the best separation, and 2 groups can be separated; that is, tumor versus healthy regions, which is in line with the histologic data (Figure 2C). A zoom of the most-separated ions from the PC1/PC2 plot is presented in Figure 2D, and a group of

Table 2. Molecular masses of known ovarian cancer protein biomarkers and masses found by MALDI MSI after using the HFIP high-mass protein preparation procedure compared to molecular masses of previously identified ovarian cancer markers.

Protein Name	Mw (Da) MALDI MSI with high mass procedure	Mw (Da) Protein previously identified in OVC	References
Tetranectin (CAA45860)	17 775	17 776	[67–70]
Neutropil Gelatinase-associated lipocalin precursor	22 576	22 571	[71]
Plasma retinol-binding protein precursor	22 986	22 990	[72]
Metalloproteinase inhibitor 1 precursor	23 152	23 153	[73]
Kallikrein 5 Precursor	26 842	26 838	[74]
Isoform 1 of Urokinase plasminogen activator surface receptor precursor	36 940	36 949	[75,76]

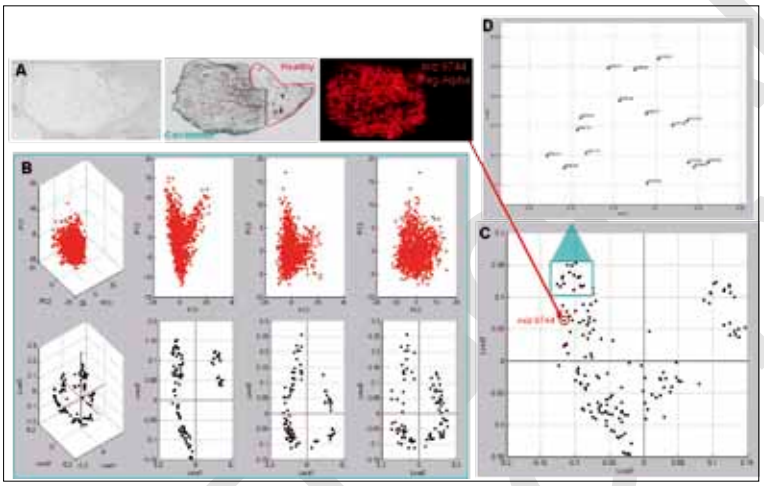

Figure 2. MALDI MSI analyses of a mucinous adenocarcinoma stage IV. (**A**) mucinous ovarian carcinoma section containing tumor and healthy parts submitted to automatic matrix deposition using a micro-spotter (CHIP-1000, Shimadzu). Location of the C-terminal part of Reg-alpha (m/z 9744) biomarker confirming the location of the tumor portion of the biopsy slice. (**B**) PCA analyses though PC1, PC2 and PC3 of the mucinous ovarian carcinoma. (**C**) Statistical PCA analyses with PC1 as tumor and PC2 as healthy tissue. Location of tumor biomarker vs protein present in the healthy part. (**D**) Zoomed view of the most-differentiated m/z corresponding to part of the specific tumor biomarkers.

specific biomarkers was detected. Their locations in the tumor region are presented in Frank et al. (2009) [33]. From the PCA results, we detected a fragment of the (PSME 1: Proteasome activator complex subunit 1, named the Reg alpha fragment), previously identified [20], is present in the cancer group with other biomarkers and not present in healthy tissue.

Biomarker identification

From the list of biomarkers detected by PCA analyses, we detect the ion at m/z of 9744, which corresponds to the fragment C-terminal of Reg alpha [20]. We validate it here through MSI (Figures 2A, 3A,B), immunocytochemistry (Figure 3C,F), Western blot (Figure 3D), and molecular biology (Figure 3E) confirmed its specificity to ovarian carcinoma. Ion at m/z of 9744 corresponding to the C-terminal part of PSME1 is detected in the carcinoma area by MSI (Figure 3A,B), which is confirmed by immunocytochemistry, with an antibody raised against the C-terminal part of the protein (Figure 3C). Western blot analyses of benign and carcinoma samples were performed either with an antibody raised against the N-terminal of PSME1 or the 1 directed against the C-terminal part (Figure 3D).

The data reflect the antibody raised against the N-terminal part recognizes the protein in both carcinoma and benign samples, whereas the antibody raised against the C-terminal recognizes its epitope only in carcinoma samples, which is in line with previous data [20] and the immunocytochemical results (Figure 3F). Figure 3F shows that this C-terminal fragment is over-present in epithelial cells of carcinoma (Figures 3F a, b, e, i). It can be detected in endometrioid nondifferentiated (Figure 3F c) or differentiated (Figure 3F a) carcinoma, sero-mucinous adenocarcinoma (Figure 3F e), and clear-cell adenocarcinoma (mesonephroma) (Figure 3F i). In benign tissues, the immunolabeling is also at the level of the epithelial cells, but more nucleus than in carcinoma can be observed in (Figures 3F f, h) the adenofibromatous tumor (Figure 3F g). All together, the data is in line with the transcriptomic results performed on the SKOV-3 epithelial carcinoma cells (Figure 3E), confirming overexpression of PSME1 gene in this carcinoma cell line. These data confirm that Reg-alpha is a specific ovarian biomarker. We recently discovered it in ascites liquid (data not shown).

For the other biomarkers detected by PCA analyses, we could detect that some have already been found in genomic

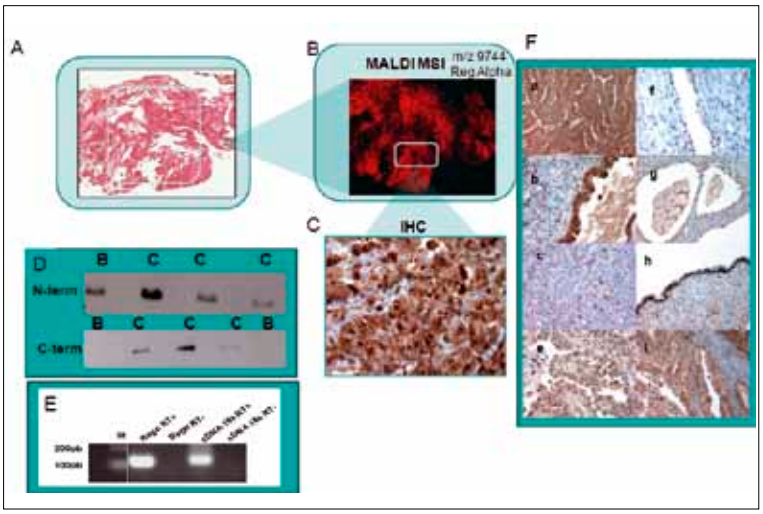

Figure 3. (**A**) Ovarian carcinoma section stained with Hematoxilin, Eosin, Safran (H&S) colorants. (**B**) MSI image of the ion at m/z: 9744, reg alpha fragment. (**C**) Immunocytochemical analyses with antibody raised against the C-terminal fragment on stage IV carcinoma sections. Most of the epithelial cells are labeled. (**D**) Western blot analyses with benign (**B**) or carcinoma from different patients (**C**) with antibodies directed against either the N-terminal or C-terminal parts of PSME1. (**E**) RT-PCR analyses of PSME1 of mRNA extracted from SKVO3. (**F**) Immunocytochemical studies with polyclonal antibody raised against the c-terminal part of Reg alpha. (a) Epithelial cells of immunolabeled differentiated endometrioid carcinoma, (b) Epithelial cells of immunolabeled in carcinoma region. (c) Cytoplasmic epithelial cells immunolabeling of nondifferentiated endometrioid carcinoma. (d) Epithelial cells of immunolabeled in clear cells adenocarcinoma (mesonephroma). (e) Nuclear epithelial cells immunolabeling of benign tumor. (f) Nuclear epithelial cells immunolabeling of adenofibromatous tumor. (g) Nuclear epithelial cells immunolabeling of seromucous area in benign tumor. (h) Cytoplasmic epithelial cells immunolabeling of sero-mucinous adenocarcinoma.

studies, and share the same mass, for example, protein S100-A12 (m/z 10568) and apolipoprotein A1 (m/z 10155) [34]. We decided to remove the MALDI matrix from the slides through a washing procedure and analyze samples by MALDI before and after trypsin digestion [32] (Figure 4). The differentiated ions then were subjected to MS/MS analysis by MALDI before analysis by nanoLC-IT/MS in MS/MS mode. For example, the ion at m/z 1160.5 detected by MALDI in a patient sample after trypsin digestion (Figure 4) was subjected to MS/MS analysis (Figure 5A). The obtained sequence of WFYIASAFR with a score of 42 (Figure 5B) was confirmed by the IT-MS/MS data, and it belongs to orosomucoid 1. Five others fragments were characterized and gave 30.3% sequence coverage (Figure 5B). The presence in the biopsy of the mRNA coding for this protein was confirmed by RT-PCR from patient with ovarian carcinoma (Figure 5C). A 150-bp fragment coding for orosomucoid was amplified (Figure 5D). Similarly, RT-PCR performed on RNA extracted from SKOV-3 epithelial carcinoma cells confirmed the expression of the orosomucoid (Figure 5E), further supporting the biochemical data. Finally, antibodies raised against the C-terminus of Reg alpha and a monoclonal against orosomucoid were used for immunocytochemistry using the specific MALDI imaging procedure [28] (Figure 5F). Both biomarkers were detected using the

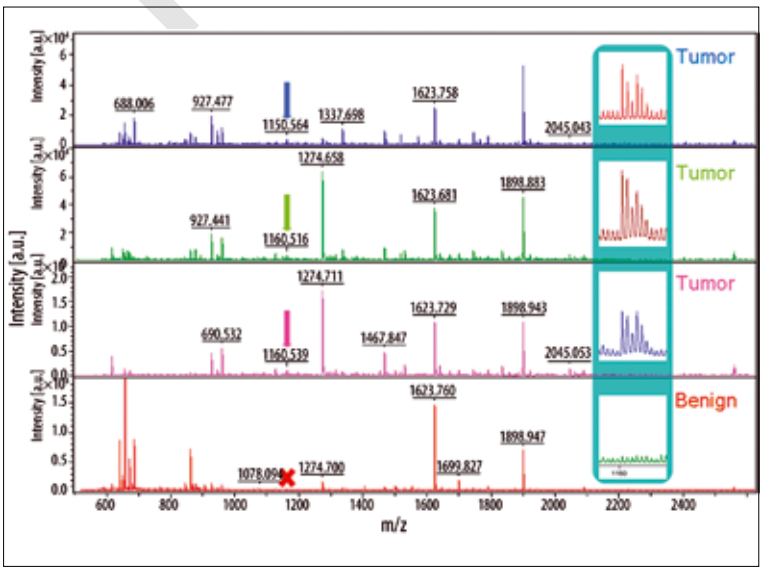

Figure 4. MALDI-MS profiles of 3 ovarian carcinomas after tissue trypsin digestion using an automatic micro-spotter (CHIP-1000, Shimadzu) versus benign tumor; a zoom of the peptide 1160.5 is performed. This peptide is present in 3 ovarian carcinomas and absent in the benign tumor. (Inset corresponds to the zoom of the 1160.5 region.)

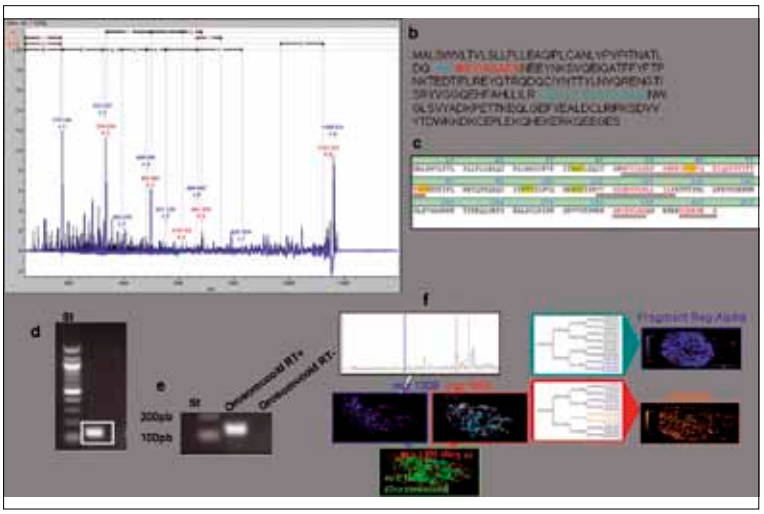

Figure 5. (**A**) MALDI MS/MS sequencing of 1160.5 using MALDI TOF-TOF. (**B**) Sequence (WFYIASAFR) in red corresponding to the fragment identified by MS-MS and localized in the orosomucoid-1 protein. (**C**) Sequence of the orosomucoid obtained by nano-LC-ITMS after trypsin digestion and by tissue MALDI TOF/TOF analyses. (**D**) RT-PCR amplification of orosomucoid from mRNA extracted biopsy (5 carcinoma versus 5 benign). (**E**) RT-PCR amplification of orosomucoid from SKOV-3 cell lines. (**F**) (a)MALDI specific imaging using the TAG-MASS concept with a polyclonal anti-Ct Reg alpha antibody tagged with a reporter (with a mass of 1309) and a monoclonal anti-orosomucoid tagged with another reporter (with a mass of 1569). (b) Merge of specific MALDI imaging molecular images of the C-terminal fragment of Reg alpha and orosomucoid. (c) MALDI imaging molecular images of the C-terminal fragment of Reg alpha and orosomucoid with the correspondence of the 2 subclass's location in the tumor part; each biomarker is characteristic of 1 region.

tag-mass procedure in the carcinoma region with specific localization (Figure 5F b), which was consistent with the clustering distribution (Figure 5F c).

A combination of MALDI TOF-TOF and nanoLC-IT MS/MS analyses (Table 3) allowed us to characterize 15 biomarkers (Table 3) from 20 samples (10 patients with ovarian cancer and absent in 10 benign tumors). Some of these have been previously reported as secreted proteins in large-scale analyses of human plasma from ovarian cancer patients [35], human ovarian cancer tumors [36] or ovarian ascites analyses [37]. Moreover, their location was determined by MSI using a bottom-up strategy. After tissue trypsin digestion, proteins were reconstructed based on their *in silico* trypsic digested peptides detected on the digested tissue (Table 4, Figure 6). MALDI imaging mass spectrometry images from digested fragments for the same protein were cumulative and gave the molecular image of its

Table 3. Biomarkers identified by nanoLC-IT-MS in MS/MS mode from 10 patients with ovarian cancer absent in 10 benign tumors.

Access number	Protein name	Molecular mass	Mascot score (average)	Sequence coverage (average)
P08670_CHAIN_0	Vimentin	53651	89.6±22.3	27±10%
P51884_CHAIN_0	Lumican Precursor	38428	63.6±5.7	19.3±4%
P02647_CHAIN_1	Apolipoprotein 1	11183	49.9±4	21.6±4.9%
P51888_CHAIN_0	Prolargin	43809	52.5±0.7	17±0.8%
Q12889_CHAIN_0	Oviductin (mucin-9)	75372	47.8±1.3	13.3±1.2%
Q01995_CHAIN_0	Transgelin	22610	49.5±2.48	26±2.44%
P02765	Orosomucoid	23511	45±2.44	20.8±1.8%
P02787_CHAIN_0	Siderophilin	77049	38.1±2.2	12±4.8%
P01009_ISOFORM_2	Alpha 1 antiprotease	39066	29.8±1.6	21±3.2%
P08727	Cytokeratin 19	44635	29.3±1.75	10±1.6%
P30086_CHAIN_0	Phosphatidyl Ethanolamine Binding Protein	21056	28.1±0.9	23±2%
P31949	Protein S100 A11	11740	22.6±0.25	24. 5±0.5%
P02790_CHAIN_0	Hemopexin	51676	21.0±0.4	6.5±1.2%
P07737_CHAIN_0	Profilin -1	15054	18.3±0.9	15.4±4.7%

Table 4. Trypsic digested fragment of proteins identified by NanoLC-IT-MS in MS/MS and found on tissue after bottom-up strategy and characterized by MS/MS.

Orosomucoide		Oviductal glycoprotein 1		Alpha anti-protease 1	
Mass	**Fragment**	**Mass**	**Fragment**	**Mass**	**Fragment**
1160.59	WFYIASAFR	1118.68	FIASVISLLR	1015.6	SVLGQLGITK
1559.83	ITGKWFYIASAFR	1120.6	LIMGIPTYGR	1110.59	LSITGTYDLK
1752.83	YVGGQEHFAHLLILR	1288.62	FTTMLSTFANR	1568.78	ECGGVFTDPKGIFK
		1248.54	SSAYAMNYWR		
		1508.77	TLLSIGGWNFGTSR		
Siderophilin		**Reg alpha C-terminal**		**Profilin-1**	
Mass	**Fragment**	**Mass**	**Fragment**	**Mass**	**Fragment**
1577.8	TAGWNIPMGLLYNK	1500.98	QLVHELDEAEYR	1643.9	TFVNITPAEVGVLVGK
		1518.2	IEDGNNFGVAV QEK	1470.7	SSFYVNGLTLGGQK
Prolargin		**Transgelin**		**Hemopexin**	
Mass	**Fragment**	**Mass**	**Fragment**	**Mass**	**Fragment**
1064.59	SFPNLAFIR	1204.7	TLMALGSLAVTK	1141.58	GGYTLVSGYPK
1309.7	LPGLVFLYMEK	1530.7	TDMFQTVDLFEGK	1120.599	NFPSPVDAAFR
1352.71	NQLEEVPSALPR	1221.62	QMEQVAQFLK		
1549.856	NLMQLNLAHNILR				
Vimentin		**S100**		**Lumican**	
Mass	**Fragment**	**Mass**	**Fragment**	**Mass**	**Fragment**
1254.5	LGDLYEEEMR	1060.48	DGYNYTLSK	1178.63	LKEDAVSAAFK
1169.70	ILLAELEQLK	1849.89	TEFLSFMNTELAAFTK	1024.55	FNALQYLR
1428.7	SLYASSPGGVYATR			1297.66	SLEDLQLTHNK
1533.84	KVESLQEEIAFLK			1180.65	RFNALQYLR
1570.88	ISLPLPNFSSLNLR				
Cytokeratin 19		**Phosphatidylethanolamine-binding**		**Apolipoprotein 1**	
Mass	**Fragment**	**Mass**	**Fragment**	**Mass**	**Fragment**
1064.09	SFPNLAFIR	1560.8	LYTLVLTDPDAPSR	1031.51	LSPLGEEMR
1365.7	SRLEQEIATYR	1632.79	NRPTSISWDGLDSGK	1301.64	THLAPYSDELR
1389.67	AALEDTLAETEAR	1949.93	GNDISSGTVLSDYVGSGPPK	1386.7	VSFLSALEEYTK
1586.83	LEHLYLNNNSIEK			1230.7	QGLLPVLESFK

tissue repartition. Interestingly, all the detected proteins have the same location.

Discussion

These characterized proteins can be grouped into functional categories such as cell proliferation, immune response modulation, signaling to the cytoskeleton, and tumor progression.

Proteins associated with cell proliferation

The S100 protein family has been previously detected in aggressive ovarian tumors [16]. In our study, we detected S100 A11 (Table 3) and S100 A12 (PCA analyses) proteins in tumors. S100 A11 has already been detected in ovarian ascites [37]. S100 A11 (or calgizzarin) is known to regulate cell growth by inhibiting DNA synthesis [38,39]. S100 A12 is known to contribute to leukocyte migration in chronic inflammatory responses [40].

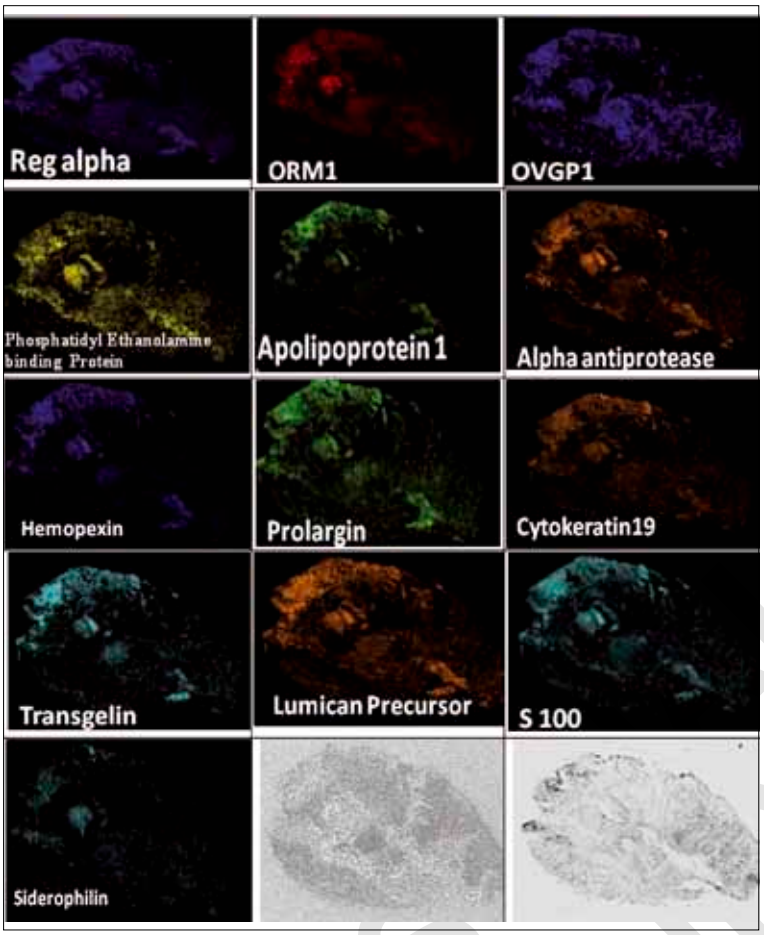

Figure 6. MALDI molecular images of the identified proteins by nanoLC-ITMS reconstructed on their trypsic digested fragment. Directly detected on tissue.

Proteins involved in immune response modulation

Recent studies have shown that ovarian cancer-associated ascites may provide an immunosuppressive environment [41]. In fact, a high CD4/CD8 ratio, which may indicate the presence of regulatory T-cells, is associated with poor outcomes. Reduced IL-2 and elevated IL-6 and IL-10 levels favor a Th2 inhibitory immune response. This immunosuppressive climate may explain the observation of non-responsiveness in ascites-derived T cells [41]. Considering these data, we tried to identify biomarkers from our pool that could be involved in such immunosuppression. In fact, we detected 5 factors involved in immune response modulation in our mucinous tumors: a C-terminal fragment of the 11S immunoproteasome (Reg-alpha), orosomucoid, apolipoprotein A1, hemopexin, and lumican.

PSME1 (proteasome activator complex subunit 1, 11S regulator complex [syn.: PA28 alpha]) cleaved into the Reg-alpha fragment could lead to default self-antigen presentation [20]. In fact, PA28 is a regulatory complex associated with 20S proteasome that consists of 3 subunits: alpha, beta, and gamma [42]. Binding of the 11S regulator complex to the 20S proteasome does not depend on ATP hydrolysis, and unlike the 19S regulatory subunit, the 11S regulator complex does not catalyze degradation of large proteins. Rather, it is responsible for MHC-class l antigen processing [43–45], which is greatly improved by interferon gamma-induced expression of the alpha and beta subunits [46].

Several viral proteins that interact with these proteasome subunits have been reported, and they may interfere with host anti-viral defenses, thereby contributing to cell transformation [47]. The manner in which they bind to the core particle via its subunits' C-terminal tails, and induce an α-ring conformational change to open the 20S gate, suggests a mechanism similar to that of the 19S particle [42]. No role in ovarian cancer has been demonstrated for the 11 S regulator complexes. Our data demonstrate a high level of expression of PA28 in carcinomas, especially in epithelial cells. The PA28 activator belongs to the antigen processing machinery (APM). Its alteration by cleavage in ovarian carcinomas may be a mechanism to evade immune recognition. Such a hypothesis has already been proposed for the case of APM chaperones such as TAP, LMP2, LMP10, and tapasin in colon carcinoma, small cell lung carcinoma, and pancreatic carcinoma cell lines. In fact, IFN-γ treatment of these carcinoma cell lines corrects the TAP, LMP, and tapasin deficiencies and enhances PA28 α, LMP7, calnexin and calreticulin expression, which is accompanied by increased levels of MHC class 1 antigens [48]. Recently, PSEM2 (proteasome activator complex subunit 2, PA28 Beta) has also been detected in ascites fluid, which implicates it in immune cell tolerance toward carcinoma cells and confirms the dysregulation of self-antigen processing in ovarian tumors [37]. Moreover, PA28 alpha seems to be a target for Epstein-Barr virus (EBV) and herpes virus (HV), as we preliminary detected by qPCR (data not shown). In fact, Pudney and colleagues [49] have shown that, as EBV-infected cells move

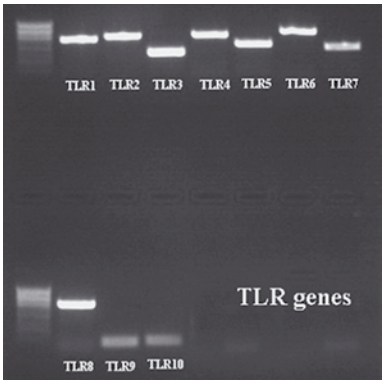

Figure 7. RT-PCR amplification of Toll-like receptors from SKOV-3 cell lines.

through the lytic cycle, their susceptibility to EBV-specific $CD8^+$ T-cell recognition falls dramatically, concomitant with a reductions in transporter associated with antigen processing (TAP) function and surface human histocompatibility leukocyte antigen (HLA) class 1 expression. Implication of virus in the cause of ovarian cancer is also sustained by the overexpression of furin enzyme (data not shown), which is known to be implicated in glycoprotein B cleavage through a motif R-X-K/R-R in both EBV and HV [50,51].

Among the 4 other factors that might participate in the tolerance phenomenon by inhibiting immune activation, the acute phase protein, orosomucoid (ORM, also known as alpha1-acid glycoprotein or AGP), is normally increased in infection, inflammation, and cancer, and it seems to have immunosuppressive properties in ovarian carcinoma ascites through inhibition of IL-2 secretion by lymphocytes [52]. Similarly, apolipoprotein A1 has been detected in conjunction with transthyretin and transferrin in early-stage mucinous tumors [53]. ApoA-I is known to decrease expression of surface molecules such as CD1a, CD80, CD86, and HLA-DR in dendritic cells, and it stimulates the production of IL-10 [54].

Interestingly, hemopexin has recently been demonstrated to reduce TNF and IL-6 from macrophages during inflammation, and it limits TLR4 and TLR2 agonist-induced macrophage cytokine production [55]. We demonstrate that in SKOV-3 epithelial ovarian carcinoma cells, all TLRs are overexpressed with the exception of TLR9 and TLR10 (Figure 7). This point is also in line with the overexpression of lumican, which is a small LRR proteoglycan in the extracellular matrix. Along with other proteoglycans, such as decorin, biglycan, and prolargin, lumican is known to be overexpressed in breast cancer and to play a role in tumor progression [56,57]. However, as demonstrated for biglycan, which interacts with TLR2/4 on macrophages [58,59], we speculate that lumican is also involved in the activation of the inflammasome through TLR2/4 interaction. The activation of all danger-sensing receptors in carcinoma cells can be explained by regulation of inflammation by carcinoma cells to facilitate tumor progression. It seems that ovarian cancer cells act as parasites and use molecular mimicry [60] to escape the immune response, and they produce immunosuppressors to achieve tolerance.

Signaling to the cytoskeleton

Several candidate proteins, including profilin-1, cofilin-1, vimentin, and cytokeratin 19 are involved in intracellular signaling to the cytoskeleton. Changes in cell phenotype, such as the conversion of epithelial cells to mesenchymal cells, are integral not only to embryonic development but also to cancer invasion and metastasis. Cells undergoing the epithelial-mesenchymal transition (EMT) lose their epithelial morphology, reorganize their cytoskeleton, and acquire a motile phenotype through the up- and down-regulation of several molecules, including tight and adherent junction proteins and mesenchymal markers. TGF-β has been described to induce EMT in ovarian adenosarcoma cells [61].

In the human lung adenocarcinoma cell line A549, this differentiation is accompanied by modification in the expression of several cytoskeleton proteins including β-actin, cofilin 1, moesin, filamin A and B, heat-shock protein beta-1, transgelin-2, S100 A11, and calpactin. These changes presumably increase migratory and invasive abilities [62]. We recently demonstrated that treatment of the ovarian cancer cell line SKOV-3 with TGF-β (10 ng/mL, 24 h) increases the expression of cofilin and profilin-1 at mRNA and protein level, and modifies its cytoskeletal organization as assessed by confocal microscopy analysis [63]. After binding to its receptor, TGF-β stimulates the reorganization of the actin cytoskeleton and triggers the formation of stress fibers and cellular protrusions [63].

Tumor progression

In conjunction with S100 proteins and cytoskeleton modifying proteins, we also detected expression of oviduct-specific glycoprotein (OGP, Mucin-9), a marker of normal oviductal epithelium. Our data are in line with that of Woo and associates, who found that OGP is a tubal differentiation marker and may indicate early events in ovarian carcinogenesis [64,65].

Conclusions

In summary, PCA and clustering, performed after MALDI imaging, analysis allow molecular tissue classification and will be of great help for pathological diagnoses. We confirmed that biomarkers detected in our tissue samples such as orosomucoid and lumican are highly glycosylated, which is in line with the mucinous phenotype of ovarian cancers. Thus, clustering analysis in conjunction with specific biomarker detection can enhance tumor tissue classification and subclassification and lead to better diagnoses. Moreover, based on the biomarkers identified in this study, we propose that ovarian cancer cells act to suppress immune responses. These findings also suggest that ovarian cancer can have a viral cause. Viruses are known to orient the immune response to immunosuppression [66]. Further studies are now in progress to explore this possibility to consider as potential biomarkers for ovarian cancer diagnosis Reg alpha fragment, mucin-9 in conjunction with oncoviral proteins specific from EBV and HHV6 viruses

Competing interests

The authors declare that they have no competing interests.

Authors' contributions

AM performed NanoLC-ITMS and MALDI imaging analyses; DB: performed PCA analyses RL and CC: performed automatic profiling studies; JF design the new ionic matrices and on tissue bottom-up strategy for biomarker identification; DV performed the EMT studies; AT carried out the molecular studies; AD performed immunocytochemistry and Western blotting, DV realized the surgeries, and the follow-up of the study; AK and RD follow-up the study though the codirection of AM and DB theses; and IF and MS conceived of the study and participated in its design and coordination. All authors read and approved the final manuscript.

REFERENCES:

1. Lambaudie E, Collinet P, Vinatier D: [Ovarian cancers and CA 125 in 2006]. Gynecol Obstet Fertil, 2006; 34: 254–57
2. Edwards BK, Brown ML, Wingo PA et al: Annual report to the nation on the status of cancer, 1975-2002, featuring population-based trends in cancer treatment. J Natl Cancer Inst, 2005; 97: 1407–27
3. Ardekani AM, Liotta LA, Petricoin EF III: Clinical potential of proteomics in the diagnosis of ovarian cancer. Expert Rev Mol Diagn, 2002; 2: 312–20
4. Bandera CA, Tsui HW, Mok SC, Tsui FW: Expression of cytokines and receptors in normal, immortalized, and malignant ovarian epithelial cell lines. Anticancer Res, 2003; 23: 3151–57
5. Conrads TP, Fusaro VA, Ross S et al: High-resolution serum proteomic features for ovarian cancer detection. Endocr Relat Cancer, 2004; 11: 163–78
6. Conrads TP, Zhou M, Petricoin EF III et al: Cancer diagnosis using proteomic patterns. Expert Rev Mol Diagn, 2003; 3: 411–20
7. Fields MM, Chevlen E: Ovarian cancer screening: a look at the evidence. Clin J Oncol Nurs, 2006; 10: 77–81
8. Johann DJ Jr, McGuigan MD, Patel AR et al: Clinical proteomics and biomarker discovery. Ann NY Acad Sci, 2004; 1022: 295–305
9. Kohn EC, Mills GB, Liotta L: Promising directions for the diagnosis and management of gynecological cancers. Int J Gynaecol Obstet, 2003; 83(Suppl.1): 203–9
10. Rapkiewicz AV, Espina V, Petricoin EF III, Liotta LA: Biomarkers of ovarian tumours. Eur J Cancer, 2004; 40: 2604–12
11. Petricoin EF, Ardekani AM, Hitt BA et al: Use of proteomic patterns in serum to identify ovarian cancer. Lancet, 2002; 359: 572–77
12. Bergen HR III, Vasmatzis G, Cliby WA et al: Discovery of ovarian cancer biomarkers in serum using NanoLC electrospray ionization TOF and FT-ICR mass spectrometry. Dis Markers, 2003; 19: 239–49
13. Diamandis EP: Proteomic patterns in serum and identification of ovarian cancer. Lancet, 2002; 360: 170; author reply 171
14. Engwegen JY, Gast MC, Schellens JH, Beijnen JH. Clinical proteomics: searching for better tumour markers with SELDI-TOF mass spectrometry. Trends Pharmacol Sci, 2006; 27: 251–59
15. Fung ET, Yip TT, Lomas L et al: Classification of cancer types by measuring variants of host response proteins using SELDI serum assays. Int J Cancer, 2005; 115: 783–89
16. Kikuchi N, Horiuchi A, Osada R et al: Nuclear expression of S100A4 is associated with aggressive behavior of epithelial ovarian carcinoma: an important autocrine/paracrine factor in tumor progression. Cancer Sci, 2006; 97: 1061–69
17. Rai AJ, Zhang Z, Rosenzweig J et al: Proteomic approaches to tumor marker discovery. Arch Pathol Lab Med, 2002; 126: 1518–26
18. Xiao Z, Prieto D, Conrads TP et al: Proteomic patterns: their potential for disease diagnosis. Mol Cell Endocrinol, 2005; 230: 95–106
19. Zhu Y, Wu R, Sangha N et al: Classifications of ovarian cancer tissues by proteomic patterns. Proteomics, 2006; 6: 5846–56
20. Lemaire R, Menguellet SA, Stauber J et al: Specific MALDI imaging and profiling for biomarker hunting and validation: fragment of the 11S proteasome activator complex, Reg alpha fragment, is a new potential ovary cancer biomarker. J Proteome Res, 2007; 6: 4127–34
21. Deininger SO, Ebert MP, Futterer A et al: MALDI Imaging Combined with Hierarchical Clustering as a New Tool for the Interpretation of Complex Human Cancers. J Proteome Res, 2008; 7(12): 5230–36
22. Walch A, Rauser S, Deininger SO, Hofler H: MALDI imaging mass spectrometry for direct tissue analysis: a new frontier for molecular histology. Histochem Cell Biol, 2008; 130: 421–34
23. Lemaire R, Wisztorski M, Desmons A et al: MALDI-MS direct tissue analysis of proteins: Improving signal sensitivity using organic treatments. Anal Chem, 2006; 78: 7145–53
24. Franck J LR, Wisztorski M, Van Remoortere A et al: MALDI mass spectrometry imaging of proteins exceeding 30000 Da. Med Sci Monit, 2010; In press
25. Holle A, Haase A, Kayser M, Hohndorf J: Optimizing UV laser focus profiles for improved MALDI performance. J Mass Spectrom, 2006; 41: 705–16
26. Lemaire R, Lucot JP, Collinet P et al: New developments in direct analyses by MALDI mass spectrometry for study ovarian cancer. Mol Cell Proteomics, 2005; 4: S305–8
27. Stauber J, Lemaire R, Wisztorski M et al: New developments in MALDI imaging mass spectrometry for pathological proteomic studies; Introduction to a novel concept, the specific MALDI imaging. Mol Cell Proteomics, 2006; 5: S247–S49
28. Lemaire R, Stauber J, Wisztorski M et al: Tag-mass: specific molecular imaging of transcriptome and proteome by mass spectrometry based on photocleavable tag. J Proteome Res, 2007; 6: 2057–67
29. Krug A, Towarowski A, Britsch S et al: Toll-like receptor expression reveals CpG DNA as a unique microbial stimulus for plasmacytoid dendritic cells which synergizes with CD40 ligand to induce high amounts of IL-12. Eur J Immunol, 2001; 31: 3026–37
30. Franck J, Arafah K, Barnes A et al: Improving tissue preparation for matrix-assisted laser desorption ionization mass spectrometry imaging. Part 1: using microspotting. Anal Chem, 2009; 81: 8193–202
31. Lemaire R, Tabet JC, Ducoroy P et al: Solid ionic matrixes for direct tissue analysis and MALDI imaging. Anal Chem, 2006; 78: 809–19
32. Fournier I, Wisztorski M, Salzet M: Tissue Imaging Using MALDI Mass Spectrometry: The New Frontier of Histopathology Proteomics Expert Review Proteomics, 2008; 5(3): 413–24
33. Franck J, Arafah K, Elayed M et al: MALDI imaging mass spectrometry: state of the art technology in clinical proteomics. Mol Cell Proteomics, 2009; 8: 2023–33
34. Hibbs K, Skubitz KM, Pambuccian SE et al: Differential gene expression in ovarian carcinoma: identification of potential biomarkers. Am J Pathol, 2004; 165: 397–414
35. Schweigert FJ: Characterisation of protein microheterogeneity and protein complexes using on-chip immunoaffinity purification-mass spectrometry. Brief Funct Genomic Proteomic, 2005; 4: 7–15
36. Bengtsson S, Krogh M, Szigyarto CA et al: Large-scale proteomics analysis of human ovarian cancer for biomarkers. J Proteome Res, 2007; 6: 1440–50
37. Gortzak-Uzan L, Ignatchenko A, Evangelou AI et al: A proteome resource of ovarian cancer ascites: integrated proteomic and bioinformatic analyses to identify putative biomarkers. J Proteome Res, 2008; 7: 339–51
38. Makino E, Sakaguchi M, Iwatsuki K, Huh NH: Introduction of an N-terminal peptide of S100C/A11 into human cells induces apoptotic cell death. J Mol Med, 2004; 82: 612–20
39. Sakaguchi M, Miyazaki M, Sonegawa H et al: PKCalpha mediates TGFbeta-induced growth inhibition of human keratinocytes via phosphorylation of S100C/A11. J Cell Biol, 2004; 164: 979–84
40. Yang Z, Tao T, Raftery MJ et al: Proinflammatory properties of the human S100 protein S100A12. J Leukoc Biol, 2001; 69: 986–94
41. Giuntoli RL II, Webb TJ, Zoso A et al: Ovarian cancer-associated ascites demonstrates altered immune environment: implications for antitumor immunity. Anticancer Res, 2009; 29: 2875–84
42. Yang Y, Fruh K, Ahn K, Peterson PA: *In vivo* assembly of the proteasomal complexes, implications for antigen processing. J Biol Chem, 1995; 270: 27687–94
43. Kloetzel PM: The proteasome system: a neglected tool for improvement of novel therapeutic strategies? Gene Ther, 1998; 5: 1297–98
44. Rivett AJ, Gardner RC: Proteasome inhibitors: from *in vitro* uses to clinical trials. J Pept Sci, 2000; 6: 478–88
45. Rotem-Yehudar R, Groettrup M, Soza A et al: LMP-associated proteolytic activities and TAP-dependent peptide transport for class 1 MHC molecules are suppressed in cell lines transformed by the highly oncogenic adenovirus 12. J Exp Med, 1996; 183: 499–514

46. Kuckelkorn U, Ruppert T, Strehl B et al: Link between organ-specific antigen processing by 20S proteasomes and CD8(+) T cell-mediated autoimmunity. J Exp Med, 2002; 195: 983–90
47. Regad T, Saib A, Lallemand-Breitenbach V et al: PML mediates the interferon-induced antiviral state against a complex retrovirus via its association with the viral transactivator. EMBO J, 2001; 20: 3495–505
48. Delp K, Momburg F, Hilmes C et al: Functional deficiencies of components of the MHC class I antigen pathway in human tumors of epithelial origin. Bone Marrow Transplant, 2000; 25(Suppl.2): S88–95
49. Pudney VA, Leese AM, Rickinson AB, Hislop AD: CD8+ immunodominance among Epstein-Barr virus lytic cycle antigens directly reflects the efficiency of antigen presentation in lytically infected cells. J Exp Med, 2005; 201: 349–60
50. Sorem J, Jardetzky TS, Longnecker R: Cleavage and secretion of Epstein-Barr virus glycoprotein 42 promote membrane fusion with B lymphocytes. J Virol, 2009; 83: 6664–72
51. Sorem J, Longnecker R: Cleavage of Epstein-Barr virus glycoprotein B is required for full function in cell-cell fusion with both epithelial and B cells. J Gen Virol, 2009; 90: 591–95
52. Elg SA, Mayer AR, Carson LF et al: Alpha-1 acid glycoprotein is an immunosuppressive factor found in ascites from ovaria carcinoma. Cancer, 1997; 80: 1448–56
53. Nosov V, Su F, Amneus M et al: Validation of serum biomarkers for detection of early-stage ovarian cancer. Am J Obstet Gynecol, 2009; 200: 639 e1–5
54. Kim KD, Lim HY, Lee HG et al: Apolipoprotein A-I induces IL-10 and PGE2 production in human monocytes and inhibits dendritic cell differentiation and maturation. Biochem Biophys Res Commun, 2005; 338: 1126–36
55. Liang X, Lin T, Sun G et al: Hemopexin down-regulates LPS-induced proinflammatory cytokines from macrophages. J Leukoc Biol, 2009; 86: 229–35
56. Leygue E, Snell L, Dotzlaw H et al: Expression of lumican in human breast carcinoma. Cancer Res, 1998; 58: 1348–52
57. Leygue E, Snell L, Dotzlaw H et al: Lumican and decorin are differentially expressed in human breast carcinoma. J Pathol, 2000; 192: 313–20
58. Babelova A, Moreth K, Tsalastra-Greul W et al: Biglycan: A danger signal that activates the NLRP3 inflammasome via toll-like and P2X receptors. J Biol Chem, 2009; 284(36): 24035–48
59. Schaefer L, Babelova A, Kiss E et al: The matrix component biglycan is proinflammatory and signals through Toll-like receptors 4 and 2 in macrophages. J Clin Invest, 2005; 115: 2223–33
60. Salzet M, Capron A, Stefano GB: Molecular crosstalk in host-parasite relationships: schistosome- and leech-host interactions. Parasitol Today, 2000; 16: 536–40
61. Kitagawa K, Murata A, Matsuura N et al: Epithelial-mesenchymal transformation of a newly established cell line from ovarian adenosarcoma by transforming growth factor-beta1. Int J Cancer, 1996; 66: 91–97
62. Keshamouni VG, Michailidis G, Grasso CS et al: Differential protein expression profiling by iTRAQ-2DLC-MS/MS of lung cancer cells undergoing epithelial-mesenchymal transition reveals a migratory/invasive phenotype. J Proteome Res, 2006; 5: 1143–54
63. Vergara D, Merlot B, Lucot JP et al: Epithelial-mesenchymal transition in ovarian cancer. Cancer Lett, 2010; 291: 59–66
64. Woo MM, Alkushi A, Verhage HG et al: Gain of OGP, an estrogen-regulated oviduct-specific glycoprotein, is associated with the development of endometrial hyperplasia and endometrial cancer. Clin Cancer Res, 2004; 10: 7958–64
65. Woo MM, Gilks CB, Verhage HG et al: Oviductal glycoprotein, a new differentiation-based indicator present in early ovarian epithelial neoplasia and cortical inclusion cysts. Gynecol Oncol, 2004; 93: 315–19
66. Wahl A, McCoy W, Schafer F et al: T Cell Tolerance for Variability in a Class I HLA Presented Influenza A Virus Epitope. J Virol, 2009; 83(18): 9206–14
67. Begum FD, Hogdall CK, Kjaer SK et al: The prognostic value of plasma soluble urokinase plasminogen activator receptor (suPAR) levels in stage III ovarian cancer patients. Anticancer Res, 2004; 24: 1981–85
68. Deng X, Hogdall EV, Hogdall CK et al: The prognostic value of pretherapeutic tetranectin and CA-125 in patients with relapse of ovarian cancer. Gynecol Oncol, 2000; 79: 416–19
69. Hogdall EV, Hogdall CK, Tingulstad S et al: Predictive values of serum tumour markers tetranectin, OVX1, CASA and CA125 in patients with a pelvic mass. Int J Cancer, 2000; 89: 519–23
70. Lundstrom MS, Hogdall CK, Nielsen AL, Nyholm HC: Serum tetranectin and CA125 in endometrial adenocarcinoma. Anticancer Res, 2000; 20: 3903–6
71. Lim R, Ahmed N, Borregaard N et al: Neutrophil gelatinase-associated lipocalin (NGAL) an early-screening biomarker for ovarian cancer: NGAL is associated with epidermal growth factor-induced epithelio-mesenchymal transition. Int J Cancer, 2007; 120: 2426–34
72. Gericke B, Raila J, Sehouli J et al: Microheterogeneity of transthyretin in serum and ascitic fluid of ovarian cancer patients. BMC Cancer, 2005; 5: 133
73. Rauvala M, Puistola U, Turpeenniemi-Hujanen T: Gelatinases and their tissue inhibitors in ovarian tumors; TIMP-1 is a predictive as well as a prognostic factor. Gynecol Oncol, 2005; 99: 656–63
74. Diamandis EP, Borgono CA, Scorilas A et al: Immunofluorometric quantification of human kallikrein 5 expression in ovarian cancer cytosols and its association with unfavorable patient prognosis. Tumour Biol, 2003; 24: 299–309
75. Pedersen N, Schmitt M, Ronne E et al: A ligand-free, soluble urokinase receptor is present in the ascitic fluid from patients with ovarian cancer. J Clin Invest, 1993; 92: 2160–67
76. Sier CF, Stephens R, Bizik J et al: The level of urokinase-type plasminogen activator receptor is increased in serum of ovarian cancer patients. Cancer Res, 1998; 58: 1843–49